Geophysical Prospecting

EAGE EUROPEAN ASSOCIATION OF GEOSCIENTISTS & ENGINEERS

*Geophysical Prospecting* doi: 10.1111/1365-2478.12075

# Aeromagnetic surveying using a simulated unmanned aircraft system

Raymond M. Caron[1]*, Claire Samson[1], Paul Straznicky[1], Stephen Ferguson[2] and Luise Sander[2]

[1]*Department of Earth Sciences, Carleton University, 1125 Colonel-By drive, Ottawa, Canada* [2]*Sander Geophysics Limited, 260 Hunt Club Road, Ottawa, Canada*

Received March 2012, revision accepted April 2013

## ABSTRACT

Carleton University and Sander Geophysics are developing an unmanned aircraft system (UAS) for aeromagnetic surveying. As an early indication of the expected performance of the unmanned aircraft system, a simulated unmanned aircraft system (sUAS) was built. The simulated unmanned aircraft system is a T-shaped structure configured as a horizontal gradiometer with two cesium magnetometers spaced 4.67 m apart, which is the same sensor geometry as planned for the unmanned aircraft system. The simulated unmanned aircraft system is flown suspended beneath a helicopter.

An 8.5 km$^2$ area in the Central Metasedimentary Belt of the Grenville Province, near Plevna, Ontario, Canada, was surveyed with the simulated unmanned aircraft system suspended 50 m above ground. The survey site was chosen on the basis of its complex geological structure. The total magnetic intensity (TMI) data recorded were compared to that obtained during a conventional fixed-wing survey and a ground survey. Transverse magneto-gradiometric data were also recorded by the simulated unmanned aircraft system.

The simulated unmanned aircraft system total magnetic intensity data have a higher resolution than the conventional fixed-wing data and were found to have a similar resolution to that of the ground survey data. The advantages of surveying with the simulated unmanned aircraft system were: (1) the acquisition of a detailed data set free of gaps in coverage at a low altitude above the terrain and (2) substantial saving of time and effort.

In the survey site, the 4.67 m simulated unmanned aircraft system gradiometer measured the transverse magnetic gradient reliably up to an altitude of 150 m above ground.

**Key words:** Magnetics, Acquisition, Imaging.

## INTRODUCTION

Aeromagnetic surveys are commonly flown using small manned aircraft such as the Piper Navajo or the Cessna Caravan. The altitude these surveys are flown at is determined by the topography of the survey site. Over a hazardous terrain that is forest covered, mountainous, or rugged they are flown at an altitude of approximately 100–150 m. Over flat terrain, they are flown at altitudes as low as 10 m. Campaigns in remote areas normally include pilot(s), a geophysicist and an aircraft maintenance engineer. A demand exists in oil and gas and mineral exploration for high-resolution, small-scale surveys flown at low altitudes (Barnard 2008). Unmanned aircraft systems (UAS) provide the possibility of performing such surveys, once object detection and avoidance (ODAV) technologies have become established, in hazardous terrain with only a small support crew and without exposing personnel to the risks of low-altitude flying. Other systems, such

*E-mail: rcaron@connect.carleton.ca

**Figure 1** Photograph of the GeoSurv II. It is powered by a 2-stroke 22 kW engine.

as an aircraft towed low-altitude magnetic bird, can provide alternate solutions to UAS's in similar terrain.

Over the last several years UAS technology has been applied towards aeromagnetic surveying on a commercial basis. UAS for aeromagnetic surveying are typically designed with composite non-magnetic materials in order to reduce the magnetic signature and increase the fuel-efficiency of the aircraft. They are also designed to operate with an object detection and avoidance system (ODAV). Due to the high power and computational requirements of these systems, they are still under development. ODAV systems are required in low-altitude flights in order to detect and avoid both moving and stationary objects within the flight path of the UAS. Proven ODAV systems that are robust and error free are a mandatory requirement by transportation authorities to approve the regular use of UAS in civilian airspace (ASUAPO AIR-160 2008; Civil Aviation Authority 2012). Until a proven ODAV system has been developed and approved by transportation authorities, the application of unmanned aerial vehicle (UAV)'s to aeromagnetic surveying are limited to areas outside of civilian airspace. This is primarily due to the restrictions placed on the operation of UAS in civilian airspace. In the United States, Canada and the United Kingdom, these restrictions include the application for a special flight operation certificate and having a remote operator within visible distance of the UAS at all times (ASUAPO AIR-160 2008; Transport Canada 2010; Civil Aviation Authority 2012).

Sander Geophysics Limited and Carleton University started collaborating in 2004 to develop a UAS for aeromagnetic surveying. In March 2010, a prototype of the UAS, the GeoSurv II, was unveiled (Samson *et al.* 2010; Caron *et al.* 2011) (Fig. 1). The GeoSurv II is a twin-boom pusher aircraft with a wingspan of 4.9 m. It is designed to sustain a cruise velocity for surveying within a range of 111–185 km/h. The airframe is made from a low-cost composite material that is manufactured using a closed cavity bag moulding variation of vacuum assisted resin transfer moulding (e.g., Maley 2008; Mahendran 2010). Non-ferrous materials are used in areas where mechanical components and fasteners are required. Steps are taken to mitigate the effect of the magnetic field created from components that contain ferrous materials, such as the engine (Samson *et al.* 2010). The UAS is not currently instrumented. The yellow pods at the wing tips are each designed to house a high-resolution cesium resonance magnetometer for total magnetic intensity (TMI) measurements. The horizontal gradiometer configuration of the cesium magnetometers will measure the transverse gradient of the Earth's magnetic field relative to the heading of the aircraft over a separation of 4.76 m. There will also be a fluxgate magnetometer in the fuselage to provide data necessary for post-processing magnetic compensation of flight manoeuvres.

While development of the GeoSurv II is continuing towards its first flight, a simulated unmanned aircraft system (sUAS) was built in late 2010. Its purpose was to evaluate the future data acquisition capabilities of the GeoSurv II, which include TMI and transverse gradient measurements (Caron 2011) and to facilitate the development of the ODAV system (Zhang, Goubran and Straznicky 2012; Boroujeni, Eternad and Whitehead 2012). The sUAS (Figs 2 and 3) is a T-shaped structure created from non-ferrous materials that replicates the gradiometer sensor geometry of the UAS. The sUAS is

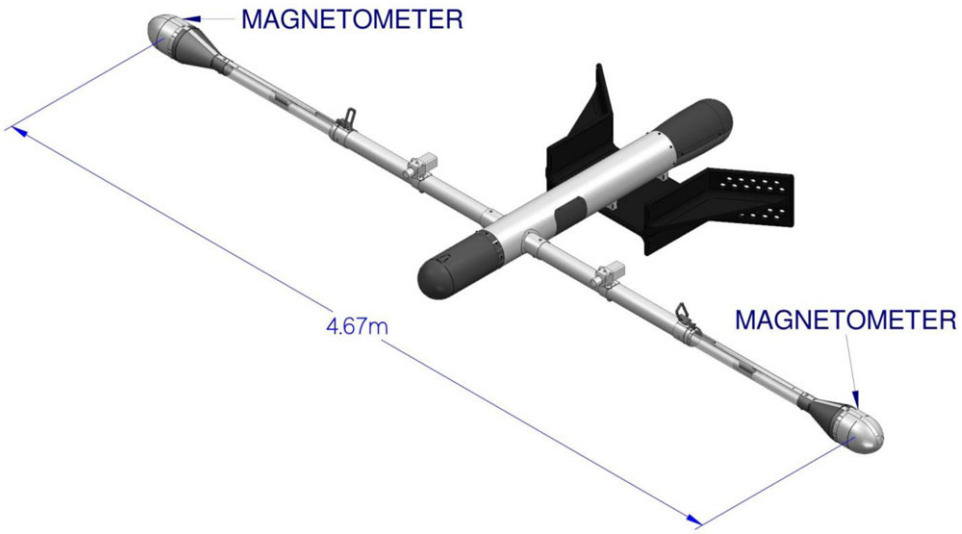


**Figure 2** Concept drawing of the sUAS. Fixtures for component testing, such as for the video camera used in the object detection and avoidance system, can be found internally and externally along the tubes separating the magnetometer pods, and within the central body of the magnetic bird.

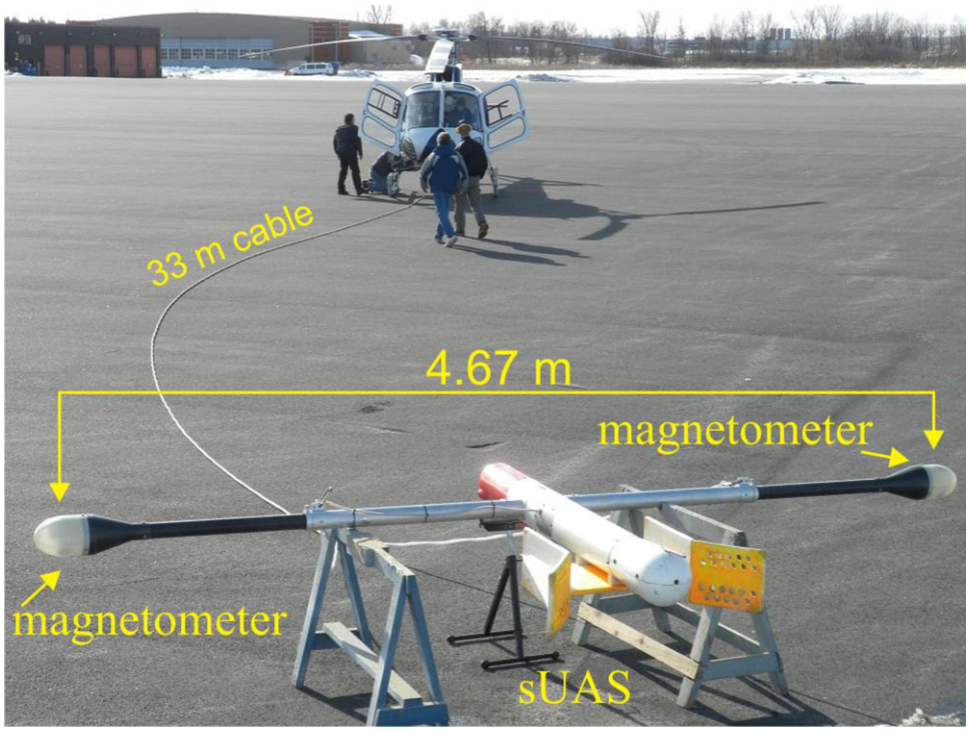


**Figure 3** sUAS being prepared for a test flight. The magnetometer pods are each loaded with a Geometrics G822-A cesium resonance magnetometer.

suspended 33 m beneath a helicopter, to reduce the magnetic interference created by the helicopter to a negligible level, and records the Earth's magnetic field 50 m above ground level, which is the nominal altitude that the UAS is designed to achieve. The sUAS is designed to resist changes in orientation during flight.

Research on the magnetic signature of the GeoSurv II was conducted in parallel (Forrester 2011; Forrester *et al.* 2011).

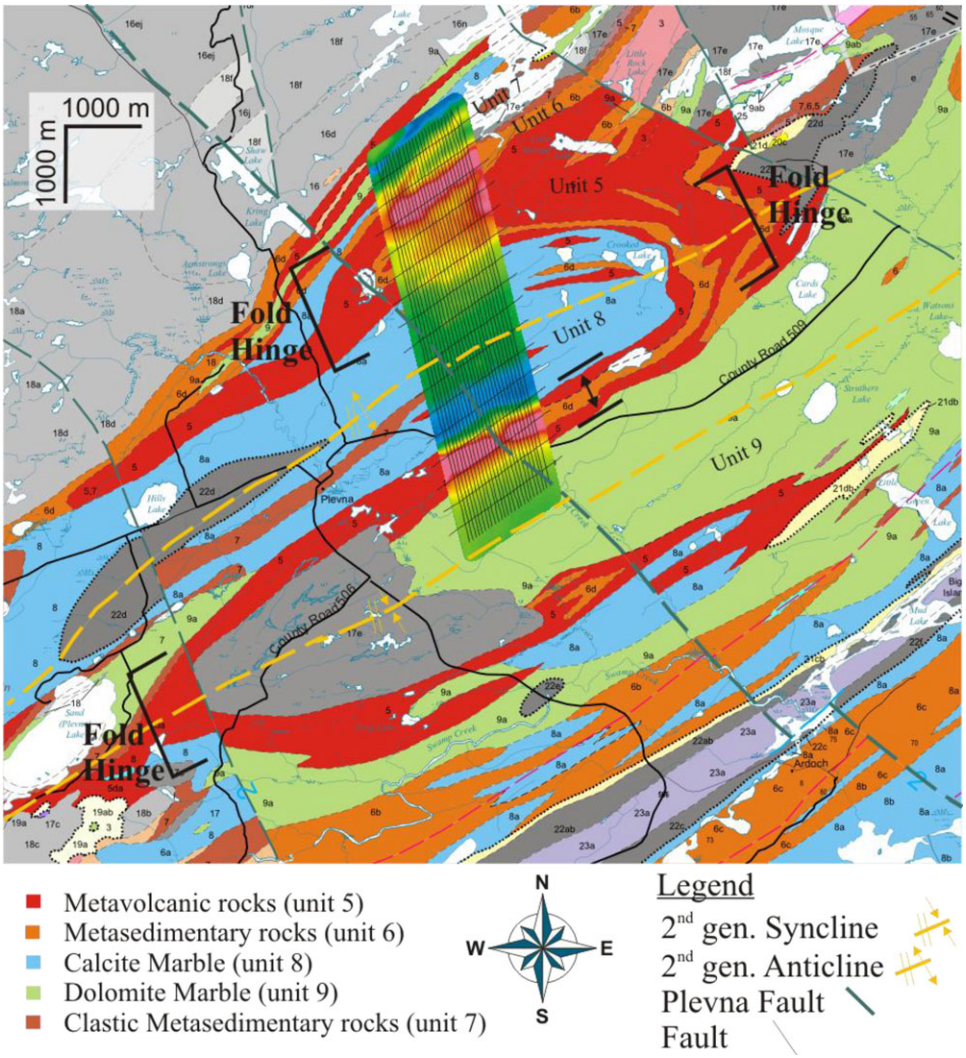


**Figure 4** sUAS TMI map superimposed on the structural geology map (modified from Easton 2006b) in the vicinity of the survey site. The sUAS traverse and control flight lines are shown in black.

The transient and static sources of magnetic noise produced by the GeoSurv II were measured using two Geometrics G822-A cesium magnetometers located in the pods at each wingtip, in a magnetically quiet environment.

The focus of this paper is to explore the feasibility of using a sUAS as a tool to measure the Earth's magnetic field. The primary objective is to determine the ability of the sUAS to detect fine magnetic details created from geological structures and to compare its performance against conventional industry benchmarks provided by fixed-wing aircraft and ground magnetic surveys. A secondary objective is to determine if the magnetic gradiometer configuration being designed for the GeoSurv II is capable of recording the transverse gradient of the Earth's magnetic field at the altitude at which the UAS is designed to survey. This will be done by comparing the observed gradiometer data, acquired by the sUAS, with TMI calculated gradient data. As the sUAS is used as a proxy to evaluate the future capabilities of the GeoSurv II, the results of these two objectives are considered to be an indication of its expected performance. Finally, another objective is to assess the level of magnetic noise generated by the GeoSurv II to establish goals for improvements.

## SURVEY SITE

The survey site is an 8.5 km$^2$ area in the Mazinaw terrain of the Central Metasedimentary Belt of the Grenville Province and is situated near the town of Plevna, Ontario, Canada (Easton

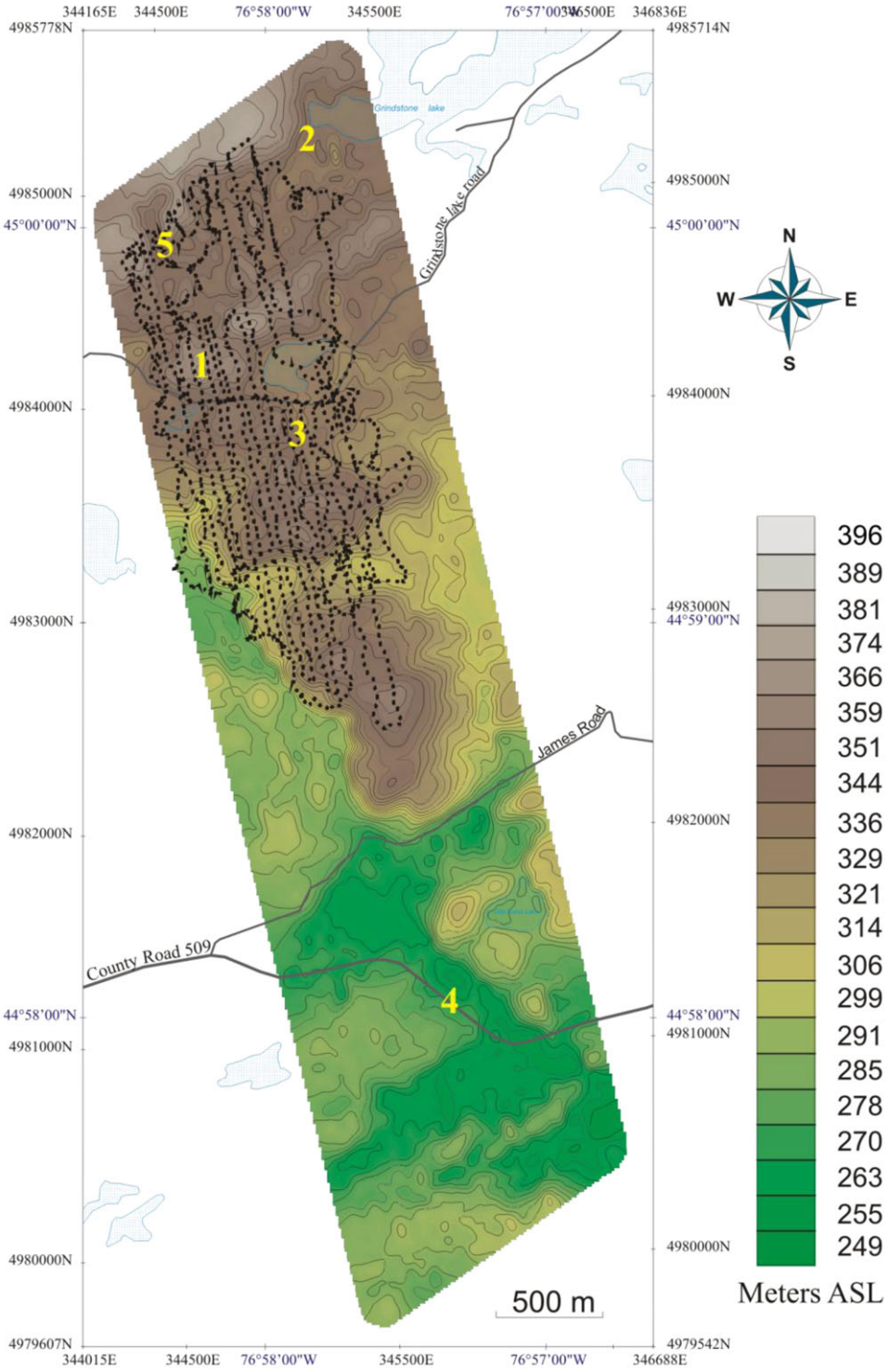


**Figure 5** DTM of the survey site. Colour scale shows terrain relief above mean sea level. The path covered by the ground survey is shown in black.

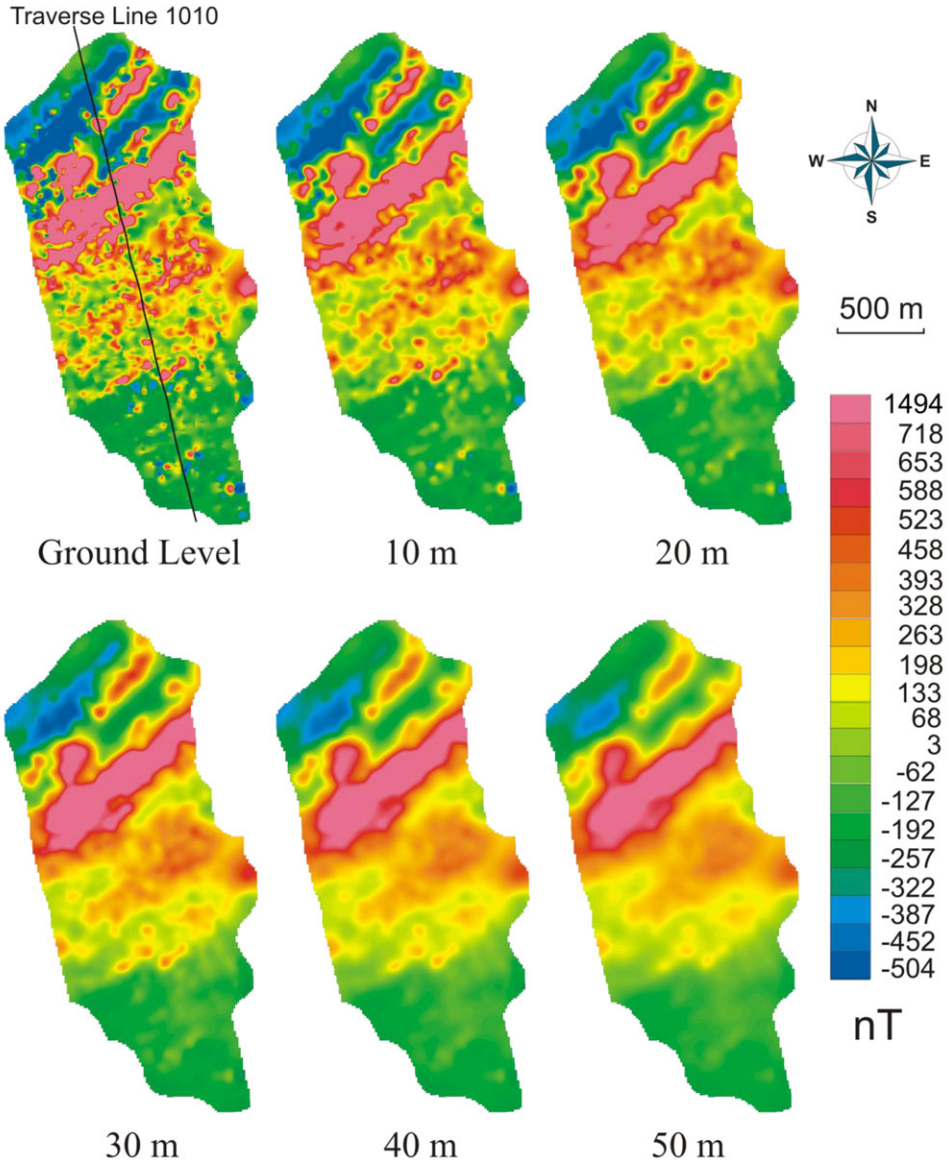


**Figure 6** TMI ground survey maps that have been progressively upward continued from ground level to an altitude of 50 m in increments of 10 m.

2006b). The site meets two criteria: (1) it features a geological structure exhibiting complexities at different scales and (2) it had been surveyed previously with a fixed-wing aircraft, for comparison purposes.

The terrain in the survey site is rugged, with 70% of the surface having a topographic gradient of 10–100 m/km and another 17% having a gradient that exceeds 100 m/km. The survey site is covered by a forest with a combination of both coniferous and deciduous trees that have respective average heights of approximately 20 and 25 m. There are also several small lakes, streams and bogs of various sizes. Outcrops and glacial erratics are common. There are some minor sources of cultural magnetic noise such as cottages and power lines.

The structural geology in the vicinity of the survey site (Fig. 4) is complex. It features a major fold that is an interference pattern created by two separate generations of folding due to tectonic events (Easton 2006a). The true nature of this fold is unknown but it is thought to be an upright tight or horizontal isoclinal fold. The portion of the fold surveyed is known as the Plevna antiform and is the northern counterpart of the Plevna synform to the south (Easton 2006a). The fold is composed of metasedimentary rocks (unit 6) inter-bedded

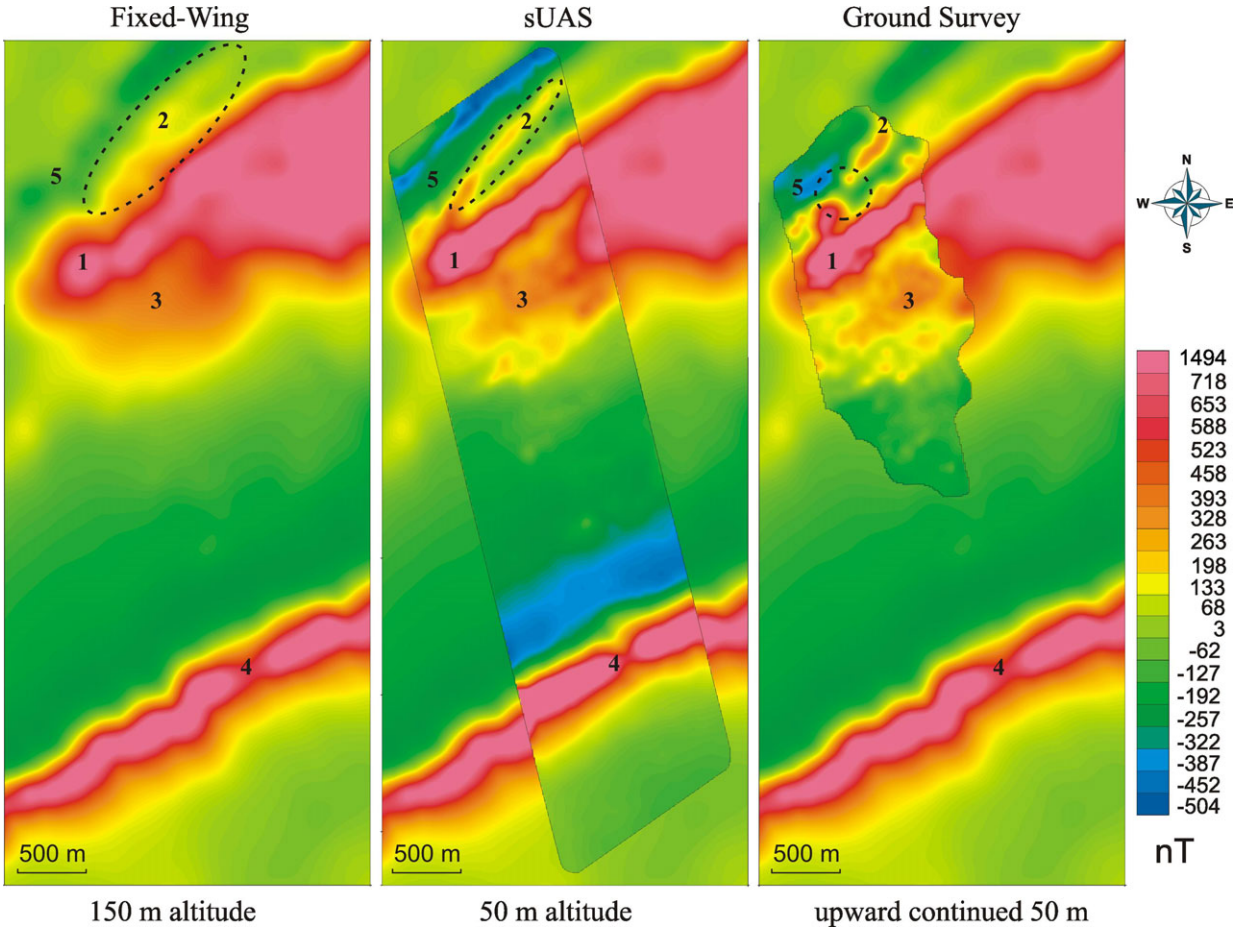


**Figure 7** Comparison of total magnetic intensity maps from the fixed-wing (gridded with a 40 m cell size) (left and background), sUAS (gridded with a 10 m cell size) (center), and upward continued to 50 m (UP50m) ground (right) surveys. Note that the slight misalignment of features 1 and 4 is due to the unavailability of GPS geo-referencing during the fixed-wing survey in 1983.

with strongly magnetic metavolcanic rocks with magnetite prophyroblasts (unit 5). These two rock types are juxtaposed against weakly magnetic calcite (unit 8) and dolomite (unit 9) marbles. Unit 7, in the north-eastern corner of the map, is a clastic metasedimentary rock that shares some characteristics with unit 6. The magnetic susceptibilities of units 6 and 7 are unknown but are stronger than units 8 and 9.

The survey site is also crossed by the Plevna fault (Fig. 4), which is a major structural feature. It has a strike that varies between azimuths of 290–320° (Black and Rencz 1987). It has no magnetic signature in the vicinity of the survey site (Pauk 1982).

## DATA ACQUISITION

Two surveys were carried out as part of this project. The first survey (February 2010) completed 160 km of surveying lines in approximately 2 hours, using the simulated unmanned aircraft system (sUAS) deployed at a nominal altitude of 50 m. Weather consisted in a clear sunny day with an occasional light breeze that did not exceed 4 km/h. The second survey conducted over two separate weeks in February and November 2010, to reduce the chance of global positioning system (GPS) interference by a forest canopy and to traverse lakes, measured the magnetic field at ground level. The ground survey covers a 2 $km^2$ northern portion of the survey site, completed in a priority basis due to surveying time constraints. The ground survey was completed at a rate of 0.6 km/h due to poor weather, GPS complications with loss of lock and impassable and rugged terrain. The sUAS and the ground surveys were conducted with 50 m traverse line spacing. In 1983, a conventional fixed-wing TMI survey was flown in the area for the Ontario Geological Survey at an altitude of 150 m, with 200 m line spacing.

## RESULTS AND DISCUSSION

### Digital terrain model

A digital terrain model (DTM) was assembled using the radar and laser altimeter measurements taken from the helicopter during the simulated unmanned aircraft system survey. As the measurements were taken during the winter, the altimeters did not detect the leafless deciduous trees but did measure coniferous trees. The presence of each coniferous tree was removed using a band-pass filter that identified individual trees by their average size. The average coniferous tree was up to 20 m tall and 5 m wide.

The DTM of the survey site (Fig. 5) aids in the interpretation of the total magnetic intensity and gradient maps. The features marked by the numbers 1–5 will be referred to throughout the following subsections. Feature 1 indicates the location of a linear topographical ridge that is striking to the north-east. Features 2 and 5 create a valley that runs between the feature 1 ridge and another ridge in the northernmost section of the map. Feature 3 indicates the location of a variable terrain that has a large number of hills. Feature 4 is the topographic expression of the Plevna Fault.

### Total magnetic intensity

The TMI map created from the 50 m altitude sUAS survey data is consistent with the structural geology map (Fig. 4). The prominent magnetic highs and lows correspond to the metavolcanic rocks of unit 6 and the marble rocks of units 8 and 9, respectively. Contrasting colours clearly delineate the location of the fold hinge and the fold limb.

The TMI map created from the ground survey data is not as extensive as that of the sUAS survey due to the difficulties involved in traversing the rugged terrain (Fig. 5). A sequence of upward continuations applied to the TMI ground survey data from ground level to an altitude of 50 m illustrates the change in frequency content in the data with increasing altitude (Fig. 6). At ground level, the data exhibit many bull's-eye anomalies. Many of these anomalies are created from localized heterogeneities. They are indistinguishable from spurious data introduced when the surveyor fell or slipped due to the rugged nature of the terrain. The widespread occurrence of these features and the ambiguity of their origin complicate interpretation by cluttering the map. As altitude increases, high frequencies are attenuated to reveal more meaningful magnetic trends that originate from deeper sources.

A comparison of the fixed-wing, sUAS and upward continued to 50 m (UP50m) ground data highlights the similarities between the TMI maps (Fig. 7). In all three cases, the magnetic high of the fold hinge (feature 1) can be found easily on each map, situated between the magnetic lows that correspond to marble units 8 and 9. Also obvious is the expected increase in resolution at lower altitude. The sUAS and UP50m maps are each showing a higher level of detail compared to the fixed-wing map. The most prominent example of the increase in resolution can be seen by comparing feature 1. Other examples are features 3 and 5, which were identified on the DTM as hills and valleys, respectively and that are now captured in finer detail.

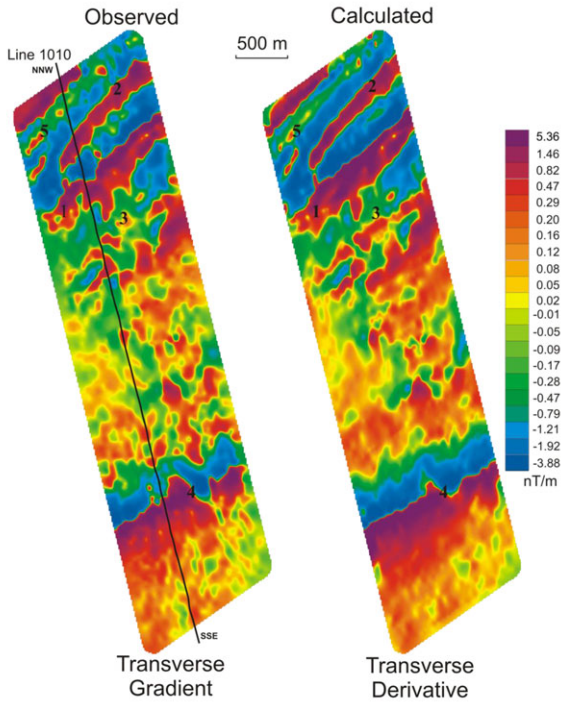


**Figure 8** Comparison between the observed transverse gradient recorded directly by the sUAS (left) and the transverse derivative calculated from the sUAS TMI map (right). The black line corresponds to traverse line 1010 shown in Figure 13.

Comparing the sUAS and UP50m TMI maps (Figure 7) reveals a key benefit of aeromagnetic surveying over ground surveying. There is a linear magnetic high identified by feature 2 and outlined by a dotted line in the maps. In the UP50m map, this feature appears boudinaged as opposed to linear due to a 75 $m^2$ gap in the original ground survey data. This gap corresponds to the location of a bog that was not traversed for safety reasons. During the computation of the map, the missing data were interpolated and the feature was not well represented. This could lead to an inaccurate interpretation of the magnetic trend and the geology in the area.

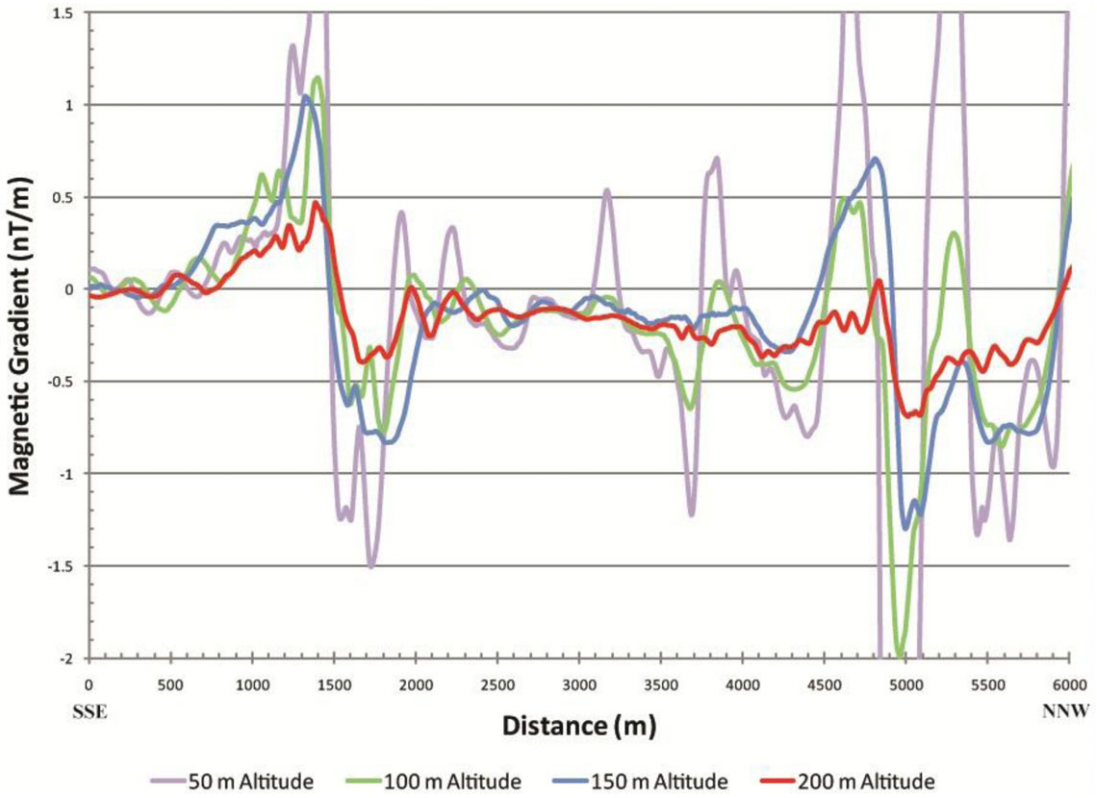


**Figure 9** Observed transverse gradient measured at different altitudes along traverse line 1010. The same drape was followed at each of the altitudes.

Further comparison between the sUAS TMI map (Fig. 7, centre) and the different upward-continued ground survey TMI maps (Fig. 6) reveals that the sUAS data are not missing magnetic trends. Features 1 and 2 are resolved to a similar extent and feature 3 has increased definition. This implies that, in the absence of the forest, if the sUAS survey had been conducted at an altitude below 50 m, using the same traverse line spacing, then the higher resolution data obtained would not have contributed additional value to geological interpretation.

### Transverse gradient

The main advantage of a transverse gradiometer is to resolve magnetic trends parallel to flight direction. Unfortunately, geological trends in this orientation are sparse in the survey site, except for the trace of the Plevna fault (Fig. 4). The fault could not be identified either on the observed transverse gradient data recorded by the sUAS or on the calculated transverse derivative map (Fig. 8). This is most probably due to the nature of the fault – which was found not to have an associated magnetic signature in previous studies (Pauk 1982) – rather than to a lack of sensitivity of the gradiometer. Features 1–5, on the contrary, show a clear correlation between the observed transverse gradient and the calculated transverse derivative (Fig. 8). Since the transverse derivative is created by interpolating the change in the intensity of the residual magnetic field from the total magnetic intensity map, which itself has been interpolated between survey lines, the interpolation is limited by the traverse line spacing of 50 m and results in a slight loss of resolution. The higher resolution of the observed transverse gradient map (Fig. 8, left) is subtle but appears in the small differences within each feature. The ridge corresponding to feature 1, for example, has been captured in more detail on the sUAS gradiometric data. The DTM shows that the ridge exhibits variations in slope angle and orientation, probably due to local differences in erosion rates (Fig. 5). The result is a ridge that has a general strike to the north-east but a cliff face that may jut out, or become recessed relative to the general ridge. The observed gradient map shows variations similar to those seen on the DTM. On the other hand, the transverse derivative (Fig. 8, right) shows a more uniform magnetic gradient, a representation unsupported by the DTM. The transverse derivative did not capture the character of the ridge with as much fidelity as the observed gradient.

**Table 1** Table detailing the static noise signature of the UAS at different headings along with the reduction of noise expected from the GAMSO strategy.

| Heading | Magnetic Noise (nT) | | | |
|---|---|---|---|---|
| | GeoSurv II Prototype | | GAMSO | |
| | Starboard | Port | Starboard | Port |
| N | 33.33 | −27.74 | 0.40 | −3.94 |
| NE | 46.16 | −28.99 | 0.55 | −4.12 |
| E | 47.96 | −24.38 | 0.58 | −3.46 |
| SE | 38.50 | −17.79 | 0.46 | −2.53 |
| S | 22.08 | −11.39 | 0.26 | −1.62 |
| SW | 10.60 | −10.59 | 0.13 | −1.50 |
| W | 10.00 | −14.27 | 0.12 | −2.03 |
| NW | 18.40 | −20.89 | 0.22 | −2.97 |

While this case history has demonstrated the functionality of the transverse gradiometer at a nominal altitude of 50 m above ground, unknown is the maximum altitude at which the transverse gradiometer can make reliable measurements. Figure 9 is a comparison of observed transverse gradients measured by the sUAS along traverse line 1010 at different nominal altitudes above ground. The 50 m profile, shown by a purple line, represents the observed transverse gradient shown in Fig. 8. The 100 m profile, shown in green, shows some attenuation in amplitude of the high-frequency peaks but is still able to reproduce most of the features seen along the 50 m profile. At a nominal altitude of 150 m, shown in blue, the amplitudes of the high-frequency peaks attenuate to the point that a large amount of detail is lost. The shape of the individual peaks becomes distorted as they begin to fuse with adjacent peaks. At a nominal altitude of 200 m, shown in red, only the most prominent peaks are reproduced. In summary, at the survey site, the 4.67 m gradiometer has an operational limit of approximately 150 m above ground level.

These results cannot be compared directly with the findings reported in Mushayandebvu and Davies (2006) concerning the Heli-Triax, a multi-sensor system flown at a nominal altitude of 30 m and capable of measuring directly the traverse gradient over a magnetometer separation of 3 m. The Heli-Triax was tested in the western Canada sedimentary basin where bedrock magnetic anomalies have low amplitude due to the presence of thick sedimentary bedrock that overlies

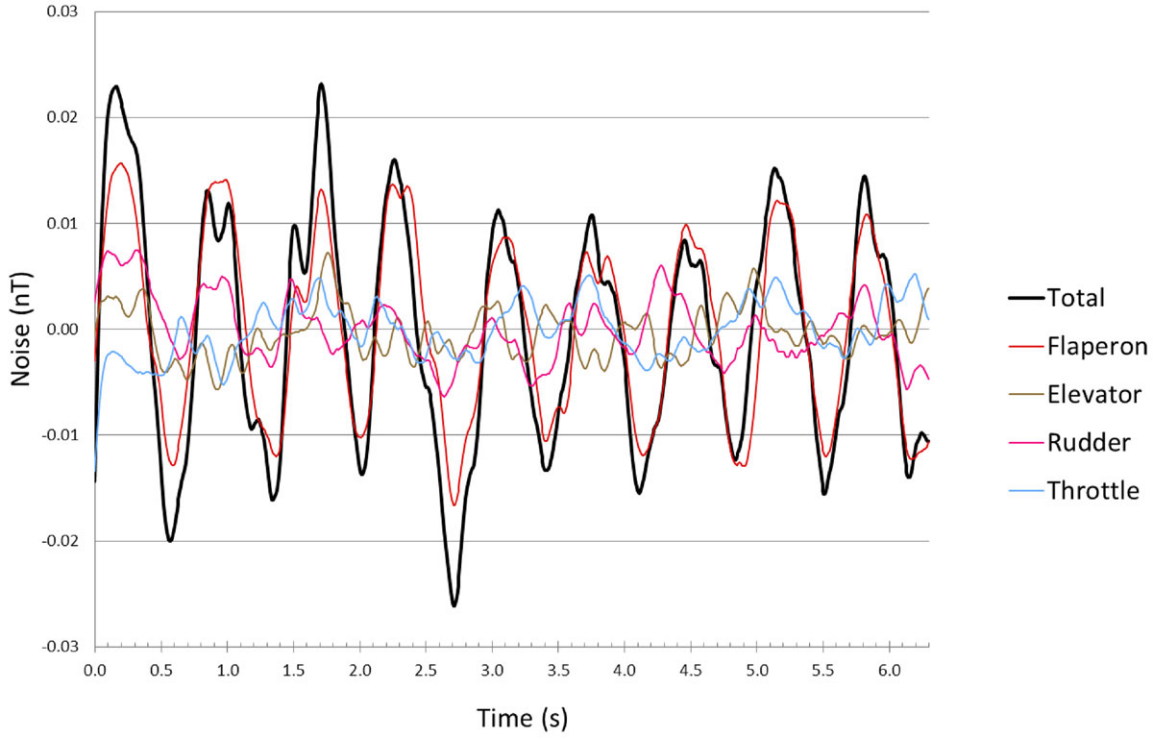


**Figure 10** Comparison of transient noise measured from servos controlling different flight control surfaces. A total of all sources has also been included to estimate the noise generated from all sources at once. These measurements were taken before the development of the GAMSO strategy.

the basement. The observed transverse gradient maps were found to be noisier than the corresponding calculated derivative maps. The noise was attributed to changes in orientation of the system during flight, which may have contributed to exceed the amplitude of the weak magnetic signature in the region. The results of the Heli-Triax system suggest that a gradiometer separation of 3 m may be insufficient to measure the transverse gradient of the magnetic field in a deep sedimentary basin. However, the sUAS results suggest that such a system is applicable to a crystalline rock environment.

### Magnetic noise

The study that evaluated the sources of magnetic noise generated by the GeoSurv II identified the servos powering the flaperons as the largest source of both static and transient noise (Forrester 2011). The noise from the servos exceeded the noise generated by both the engine and the avionics and was enough to skew the magnetic field of the aircraft to be asymmetric in nature, resulting in a higher level of noise measured at the starboard magnetometer than at the port magnetometer.

The level of static magnetic noise can be expected to change depending on the flight manoeuvres being performed by the UAS. Table 1 shows the noise produced by the GeoSurv II at different compass headings, with the largest level of noise, approximately 50 nT, found for the NE heading. Such a level of noise would be high enough to have a deleterious effect on the signal recorded during both TMI and transverse gradiometer surveying. In post-processing, a Genetic Algorithm Magnetic Signature Optimization (GAMSO) strategy reduced the noise measured by the starboard and port magnetometers by up to 98.8% and 85.8%, respectively (Forrester *et al*. 2012) (Table 1). Even after the GAMSO correction, however, the static noise level was deemed to be too high to simulate its effect on the sUAS data.

Results from a test performed to measure the transient noise generated by the servos is more encouraging (Fig. 10). The largest source of transient noise, created by the flaperon servos, did not exceed $\pm 0.017$ nT, while the sum of all sources of noise did not exceed $\pm 0.03$ nT.

## CONCLUSIONS

Visual inspection of the TMI maps created from the data gathered during the fixed-wing, ground and sUAS surveys provides a quick, qualitative assessment of the aeromagnetic surveying capabilities of the sUAS. The results presented show that the sUAS survey is able to create higher resolution TMI and gradient maps, in hazardous terrain, than a conventional fixed-wing survey, by flying at a lower altitude. The results also show that a survey does not need to be conducted at ground level in order to detect subtle geologically-significant magnetic trends. In the case history presented here, the sUAS was able to delineate all the magnetic trends that were detected during the ground survey. In addition, the sUAS survey covered the area completely in a fraction of the time taken by the incomplete ground survey and led to more reliable maps that are free from interpolation problems created from missing sections. The results also showed that the 4.67 m sUAS transverse gradiometer was able to capture all of the magnetic trends present on the calculated transverse derivative. In the survey site, it proved to be effective up to an altitude of 150 m. The signal from the sUAS TMI and the transverse gradient measurements are strong enough to overcome the transient sources of noise created by the GeoSurv II prototype. Design changes will have to be introduced to significantly reduce static magnetic noise generated by the servos.

## REFERENCES

Aviation Safety Unmanned Aircraft Program Office (ASUAPO) AIR-160. 2008. UAS interim operational approval guidance 08–01: Unmanned aircraft operations in the national airspace system. Federal Aviation Administration, Department of Transportation.

Barnard J.A. 2008. The use of unmanned aircraft in oil, gas and mineral E+P activities. *SEG Expanded Abstracts* **27**, 1132–1136.

Black S.J. and Rencz A.N. 1987. Industrial minerals in Eastern Ontario: Clarendon sillimanite occurrence. *Geological Survey of Canada, Open File* **1672**, 1–9.

Boroujeni N.S., Eternad S.A. and Whitehead A. 2012. Robust horizon detection using segmentation for UAV applications. Institute of Electrical and Electronics Engineers (IEEE). Canadian Conference on Computer and Robot Vision (CRV), May 2012.

Caron R. 2011. *Aeromagnetic surveying using a simulated unmanned aircraft system*. Master of Science thesis. Earth Sciences, Carleton University, 1–116.

Caron R., Samson C., Straznicky P., Ferguson S., Archer R. and Sander L. 2011. Magnetic and magneto-gradiometric surveying using a simulated unmanned aircraft system. *SEG Expanded Abstracts* **30**, 861–865.

Civil Aviation Authority. 2012. CAP722 Unmanned aircraft system operations in UK airspace –Guidance. Safety Regulation Group, Civil Aviation Authority.

Easton R.M. 2006a. Precambrian geology of the Cloyne-Plevna-Ompah area, northern Mazinaw Domain, Grenville Province. Ontario Geological Survey, Open File Report 5454. 1–165.

Easton R.M. 2006b. Precambrian geology, Cloyne-Plevna-Ompah area. Ontario Geological Survey, Preliminary Map P.3443, scale 1:50 000.

Forrester R.W. 2011. *Magnetic signature control strategies for an unmanned aircraft system*. Master of Applied Science thesis. Mechanical and Aerospace Engineering, Carleton University, 1–212.

Forrester R.W., Huq S.M., Ahmadi M. and Straznicky P. 2012. Magnetic signature attenuation of an unmanned aircraft system for aeromagnetic survey. Submitted to: IEEE/ASME Transactions on Mechatronics.

Mahendran M. 2010. *An improved mouldless manufacturing method for foam-core composite sandwich structures*. Master of Applied Science thesis. Mechanical and Aerospace Engineering, Carleton University, 1–168.

Maley J.A. 2008. *An investigation into low-cost manufacturing of carbon epoxy composites and a novel "mouldless" technique using the Vacuum Assisted Resin Transfer Moulding (VARTM) method*. Master of Applied Science thesis. Mechanical and Aerospace Engineering, Carleton University, 1–172.

Mushayandebvu M.F. and Davies J. 2006. Magnetic gradients in sedimentary basins: Examples from the Western Canada Sedimentary Basin. *The Leading Edge* **25**, 69–73.

Pauk L. 1982. Geology of the Ardoch area, Frontenac County. Ontario Geological Survey, Open File Report **5381**, 1–125.

Samson C., Straznicky P., Laliberté J., Caron R., Ferguson S. and Archer R. 2010. Designing and building an unmanned aircraft system for aeromagnetic surveying. *SEG Expanded Abstracts* **29**, 1167–1171.

Transport Canada. 2010. Canadian aviation regulations (CARs). Transport Canada. Section 101.01, 602.41

Zhang F., Goubran R. and Straznicky P. 2012. Obstacle detection for low flying UAS using monocular camera. Institute of Electrical and Electronics Engineers (IEEE). International Instrumentation and Measurement Technology Conference, May, 2012.